# Correlation of the Formation and the Decomposition Process of the BSCF Perovskite at Intermediate Temperatures

Mirko Arnold,*,† Thorsten M. Gesing,‡,§ Julia Martynczuk,† and Armin Feldhoff†

*Institut für Physikalische Chemie und Elektrochemie, Leibniz Universität Hannover, Callinstrasse 3-3A, D-30167 Hannover, Germany, and Institut für Mineralogie, Leibniz Universität Hannover, Callinstrasse 3, D-30167 Hannover, Germany*

*Received May 29, 2008. Revised Manuscript Received July 7, 2008*

The mixed ionic-electronic conductor (MIEC) $(Ba_{0.5}Sr_{0.5})(Co_{0.8}Fe_{0.2})O_{3-\delta}$ (BSCF) is a renowned material with applications in membrane reactors and as cathodes in solid-oxide fuel cells. Despite BSCF's large oxygen permeabilities, long-time phase instability at intermediate temperatures has been reported. However, the mechanism of this decomposition is still unclear. Here, we present a study of the synthesis of BSCF and compare our results with those obtained from long-time decomposition. Rietveld and Le Bail analysis as well as transmission electron microscopy studies were applied to investigate the reaction sequence in BSCF formation. We are now able to draw the following conclusion about the reaction mechanism: the formation as well as decomposition is due to a reversible reordering of the hexagonal $AO_3$-layer stacking sequence in the cubic perovskite, which can occur if the cubic BSCF is kept at temperatures below $T =$ 1173 K for long time periods, thereby leading to the decomposition of BSCF into a three-phase mixture. The driving force for this reaction was identified to occur at the cobalt site because cobalt prefers a low-spin configuration in the 3+ oxidation state. This reaction occurs only at temperatures below $T =$ 1173 K because of the oxidation of cobalt at low temperatures.

## Introduction

In the field of mixed ionic and electronic conductors (MIECs) with high oxygen conductivity, the $(Ba_{0.5}Sr_{0.5})(Co_{0.8}Fe_{0.2})O_{3-\delta}$ (denoted as BSCF) with cubic perovskite structure ($ABO_3$; A = alkaline earth, B = transition metal, O = oxygen) is regarded as one of the most promising materials.[1,2] MIECs with oxygen conductivity can be employed as membranes for oxygen separation[2−6] and as cathodes in solid-oxide fuel cells.[1,7,8] Exceptionally high concentrations of mobile oxygen vacancies accompanied by excellent phase stability are accountable for BSCF's large oxygen transport rates.[9] Despite its high oxygen permeability and short-term stability, other issues have to be examined in view of a BSCF's prospective industrial use.[10] Among others, the chemical long-term stability needs to be discussed because membranes are usually set up for longer time periods. Chemical instability, i.e., the decomposition of the BSCF, could lead to membrane failures (cracking) as different unit-cell volumes may occur in these phase mixtures at the same time. Secondly, decomposition is also expected to degrade the oxygen permeation fluxes, which have to be avoided in industrial applications in order to ensure smooth processes.[10]

In the year 2000[3] and much more recently,[11,12] the long-term stability of BSCF has been investigated and discussed. Shao et al. reported that BSCF undergoes structural changes if the material is kept at $T = 1023$ K under air for time periods of 500 h. They attributed the observed additional peaks in the X-ray diffraction (XRD) pattern to $BaCoO_2$.[3] Further indications of the decomposition in BSCF were observed by Rebeilleau-Dassonneville et al., who observed additional intensities (25−30° and 42.5° $2\theta$, Cu−$K_{\alpha1,2}$ radiation) in the XRD pattern if the BSCF was kept below $T = 1073$ K, but no phase attribution was provided in this study.[11] Švarcová stated that around and below a critical temperature of $T = 1123$ K, the former single cubic perovskite phase undergoes a decomposition into a hexagonal perovskite and a cubic perovskite, thus exhibiting a two-phase region.[12] Švarcová has also shown that the decomposi-

* Corresponding author. E-mail: Mirko.arnold@pci.uni-hannover.de. Phone: 0049-511-762-4896. Fax: 0049-511-762-19121.
† Institut für Physikalische Chemie und Elektrochemie, Leibniz Universität Hannover.
‡ Institut für Mineralogie, Leibniz Universität Hannover.
§ Present address: Universität Bremen, FB05 Kristallographie, Klagenfurther Strasse, D-28359 Bremen.

(1) Shao, Z. P.; Haile, S. M. *Nature* **2004**, *431*, 170.
(2) Chen, C. S.; Feng, S. J.; Ran, S.; Zhu, D. C.; Liu, W.; Bouwmeester, H. J. M. *Angew. Chem., Int. Ed.* **2003**, *42*, 5354.
(3) Shao, Z. P.; Yang, W. S.; Cong, Y.; Dong, H.; Tong, J. H.; Xiong, G. X. *J. Membr. Sci.* **2000**, *172*, 177.
(4) Caro, J.; Wang, H. H.; Tablet, C.; Kleinert, A.; Feldhoff, A.; Schiestel, T.; Kilgus, M.; Kölsch, P.; Werth, S. *Catal. Today* **2006**, *118*, 128.
(5) Ge, L.; Zhou, W.; Ran, R.; Liu, S. M.; Shao, Z. P.; Jin, W.; Xu, N. P. *J. Membr. Sci.* **2007**, *306*, 318.
(6) Zeng, P. Y.; Chen, Z. H.; Zhou, W.; Gu, H. X.; Shao, Z. P.; Liu, S. M. *J. Membr. Sci.* **2007**, *291*, 148.
(7) Lai, W.; Haile, S. *Phys. Chem. Chem. Phys.* **2008**, *10*, 865.
(8) Liu, Q. L.; Khor, K. A.; Chan, S. H. *J. Power Sources* **2006**, *161*, 123.
(9) McIntosh, S.; Vente, J. F.; Haije, W. G.; Blank, D. H. A.; Bouwmeester, H. J. M. *Chem. Mater.* **2006**, *18*, 2187.
(10) Vente, J. F.; McIntosh, S.; Haije, W. G.; Bouwmeester, H. J. M. *J. Solid State Electrochem.* **2006**, *10*, 581.
(11) Rebeilleau-Dassonneville, M.; Rosini, S.; van Veen, A. C.; Farrusseng, D.; Mirodatos, C. *Catal. Today* **2005**, *104*, 131.
(12) Švarcová, S.; Wiik, K.; Tolchard, J.; Bouwmeester, H. J. M.; Grande, T. *Solid State Ionics* **2008**, *178*, 1787.

10.1021/cm801463h CCC: $40.75 
Published on Web 08/29/2008

tion process, which occurs from annealed BSCF samples, possesses presumably the same phases as the raw powder reannealed at $T = 1023$ K, thus showing that the decomposition process is reversible.

We have already quoted that the synthetic process of BSCF may provide useful information about the decomposition as a reversible mechanism might be present.[13] We agree with Švarcová et al. that the decomposition of BSCF is characterized by the same reaction pathway as the synthetic process of BSCF because we found similar XRD patterns for the synthetic process as well as for the decomposing process. This presumption has been emphasized by comparing the XRD pattern of a reannealed cubic perovskite powder with the XRD pattern of a BSCF powder that had been interrupted in the synthetic process. At this point, we stress that Švarcová et al. obtained the same intermediate perovskites using the spray pyrolysis method as those reported using the sol−gel method. This places the presented findings about the sol−gel synthesis method in a more general context. As previously discussed, the reaction pathway of the BSCF formation via the sol−gel route can be divided into three parts.[13] The first part is the formation of a mixed barium−strontium carbonate $(Ba_{0.5}Sr_{0.5})CO_3$ and a mixed cobalt−iron spinel $(Fe_{0.6}Co_{0.4})Co_2O_4$ (the stoichiometry claims no site attribution of cobalt and iron and a real association to either tetrahedral/octahedral occupation could not be provided). The second part is the formation of an intermediate hexagonal perovskite (SG $P6_3/mmc$) and an intermediate cubic perovskite (SG $Pm\bar{3}m$). Finally, the third part is the formation of the final cubic perovskite structure at the expense of both the hexagonal as well as the cubic perovskites. However, it has been postulated by Švarcová et al. that the decomposition of the BSCF at low temperatures is due to the oxidation of the B-site cations, which yields a hexagonal perovskite, because of the fact that the smaller ionic radii favor the formation of hexagonal perovskite structures. The compositions as well as the structures formed through this decomposition process remain unknown.

The present study focuses on the second and on the third part of the synthetic process. By applying Rietveld[14] and LeBail[15] refinement procedures to examine the final parts of the reaction sequence, we are able to draw an even more detailed picture of the reaction sequence from the picture presented in our previous report. This was accompanied by performing an intensive transmission electron microscopy study combined with quantitative energy-dispersive X-ray spectroscopy (EDXS) of partly reacted powders in order to support the XRD findings.

## Experimental Section

Powders of BSCF stoichiometry were synthesised by a sol−gel reaction procedure, as reported in detail elsewhere.[3,13,16,17] To obtain partly reacted powders and avoid the complete reaction towards the BSCF, the final calcinations steps were conducted at temperatures below $T = 1223$ K. Detailed investigations of powders that had been prepared in ambient air with different dwell times in the temperature regime between $T = 923$ K and $T = 1223$ K led us to the conclusion that five phases were involved during the synthesis of the perovskite. This has also been confirmed by a previously reported in situ X-ray diffraction study.[13] Particular powders, which represent the final steps in the synthetic process, were selected in order to perform X-ray refinements as well as transmission electron microscopy (TEM) studies. In particular, two powders, one at $T = 973$ K, 10 h (sample 1) and the other $T = 1023$ K, 10 h (sample 2), were investigated using the above techniques.

For structure refinements of the product phase, the X-ray powder diffraction data was collected on a Bruker AXS D8 Advance diffractometer using a flat sample geometry, a primary Göbel mirror and Cu−$K_{\alpha 1,2}$ radiation. Additionally, a secondary graphite monochromator was used to suppress the fluorescence radiation of the sample. A total of 3750 data points were collected with a step width of 0.02° in the $2\theta$ range from 10° to 85°. Rietveld refinements on the XRD powder data were carried out by using the TOPAS 3.0 (Bruker AXS) software. During refinements, general parameters, such as the scale factor, a maximum of three or four background parameters, and the zero point of the counter, were optimized. Profile shape calculations were carried out on the basis of standard instrumental parameters using the fundamental parameter approach implemented in the program by varying also the average crystal size (integral breadth) and the strain parameter, $\varepsilon_0$. Additionally, the cell parameter and the displacement parameters were also refined. In the case of site occupation with mixed atoms, linear constraints were used for the occupancy (the occupancy of atom B is equivalent to 1.0 minus the occupancy of atom A) and the displacement parameters (atoms on the same position have the same displacement parameter).

TEM was performed at 200 kV on a field-emission instrument (JEOL JEM-2100F). The microscope was equipped with an ultra-high-resolution pole piece that provides a point-resolution better than 0.19 nm (with a spherical aberration constant, $C_S = 0.5$ mm, and a chromatic aberration constant, $C_C = 1.1$ mm) and allowed us to perform high-resolution transmission electron microscopy (HRTEM) studies. The microscope was equipped with a 1k charge-coupled-device (CCD) camera. Diffraction data were obtained by fast Fourier transformation (FFT) of the HRTEM micrographs using the Gatan Digital Micrograph software (Version 1.70.16). Quantitative elemental analysis using energy-dispersive X-ray spectroscopy (EDXS) was performed on an Oxford Instruments INCA-200-TEM system with an ultra-thin window that was attached to the microscope. A detailed description of the TEM sample preparation can be found in our previous reports.[13,16,17]

## Results

Figure 1 shows the Rietveld refinement of powder sample 1 that has been heated for 10 h at $T = 973$ K. Four phases were present, namely a mixed carbonate, a mixed spinel, a hexagonal, and a cubic perovskite. A detailed summary of the Rietveld analysis of the phase mixture can be found in Table 1. The carbonate and spinel phases were present to a minor extent (~8 %), whereas the hexagonal perovskite (~58

(13) Arnold, M.; Wang, H. H.; Martynczuk, J.; Feldhoff, A. *J. Am. Ceram. Soc.* **2007**, *90*, 3651.
(14) Rietveld, H. M. *J. Appl. Cryst.* **1969**, *2*, 65.
(15) Le Bail, A.; Duroy, H.; Fourquet, J. L. *Mater. Res. Bull.* **1988**, *23*, 447.
(16) Feldhoff, A.; Arnold, M.; Martynczuk, J.; Gesing, Th. M.; Wang, H. H. *Solid State Sci.* **2007**, *10*, 689–701.
(17) Martynczuk, J.; Arnold, M.; Wang, H. H.; Caro, J.; Feldhoff, A. *Adv. Mater.* **2007**, *19*, 2134.

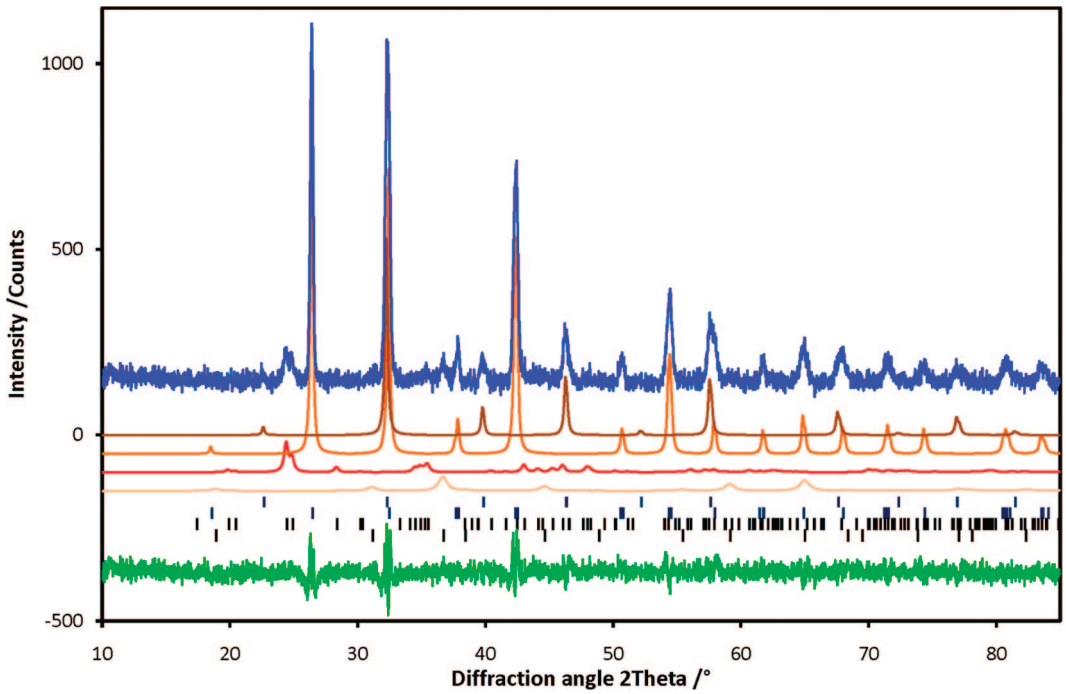


**Figure 1.** Rietveld plot of sample 1 ($T = 973$ K, 10 h). The observed (blue) and calculated intensities [brown, $(Ba_{0.25}Sr_{0.75})(Co_{0.6}Fe_{0.4})O_{3-\delta}$ (cubic-perovskite); light brown, $(Ba_{0.75}Sr_{0.25})CoO_{3-\delta}$ (hexagonal perovskite); red, $(Ba_{0.5}Sr_{0.5})CO_3$ (aragonite-modification); pink, $(Fe_{0.6}Co_{0.4})Co_2O_4$ (spinel-modification)] together with the difference (green) between the observed and calculated pattern as well as the possible reflex position (tick marks) are given.

**Table 1. Summary of the Rietveld Refinement of Sample 1 ($T = 973$ K, 10 h) and the Rietveld/Le Bail Refinement of Sample 2 ($T = 1023$ K, 10 h)**

| phase | space goup | space group ref. | lattice parameter (nm) |
|---|---|---|---|
| | | Sample 1 | |
| $(Ba_{0.5}Sr_{0.5})CO_3$ | *Pmcn* | De Villiers,[18] Kiseleva et al.[19] | $a = 0.51911(48)$, $b = 0.86708(91)$, $c = 0.62752(67)$ |
| $(Fe_{0.6}Co_{0.4})Co_2O_4$ | $Fd\bar{3}m$ | Liu et al.[20] | $a = 0.81073(42)$ |
| $(Ba_{0.75}Sr_{0.25})CoO_{3-\delta}$ | $P6_3/mmc$ | Gushee et al., [21]Taguchi et al. [22] | $a = 0.55076(4)$, $c = 0.47409(5)$ |
| $(Ba_{0.25}Sr_{0.75})(Co_{0.6}Fe_{0.4})O_{3-\delta}$ | $Pm\bar{3}m$ | McIntosh et al.[9] | $a = 0.39145(3)$ |
| | | Sample 2 | |
| $(Ba_{0.6-x}Sr_{0.4+x})(Co_{1-y}Fe_y)O_{3-\delta}$ | *P2/m* | this work | $a = 1.10307(62)$, $b = 0.97080(53)$, $c = 1.40776(92)$, $\beta = 91.6526(45)°$ |
| $(Ba_{0.6+x}Sr_{0.4-x})CoO_{3-\delta}$ | $P6_3/mmc$ | Gushee et al., [21]Taguchi et al. [22] | $a = 0.56434(50)$, $c = 0.44478(49)$ |
| $(Ba_{0.25}Sr_{0.75})(Co_{0.6}Fe_{0.4})O_{3-\delta}$ | $Pm\bar{3}m$ | McIntosh et al.[9] | $a = 0.39063(17)$ |

%) and the cubic perovskite (~25 %) were the major phases. Also, an unknown amount of amorphous phase is present.

The refinement converged to reliability factors of $R_{WP} = 9.12$ % and $R_P = 7.52$ % for the pattern with a goodness of fit = 1.17, and a Durban−Watson parameter of 1.47. We have assigned the following stoichiometries to the perovskite structures: $(Ba_{0.75}Sr_{0.25})CoO_{3-\delta}$ for the hexagonal perovskite and $(Ba_{0.25}Sr_{0.75})(Co_{0.6}Fe_{0.4})O_{3-\delta}$ for the cubic perovskite. This was in excellent agreement with the reported unit cell parameters for the cubic perovskite unit cell,[9] and the hexagonal unit cell parameters were in excellent agreement with the findings by Gushee et al. and Taguchi et al.[21,22] This is due to the fact that the unit cell of the observed hexagonal perovskite was smaller compared to that found in $BaCoO_{2.83}$, and the unit-cell parameters of the observed cubic perovskite was smaller than that reported for BSCF.

To determine the B-site stoichiometry, which is difficult to ascertain from the XRD data alone, and to confirm the A-site occupancy obtained from XRD analysis, we have conducted a quantitative EDXS study on a TEM for sample 1 (data not shown). Additionally, we successfully prepared samples of the hexagonal structure, within the series $(Ba_{1-x}Sr_x)CoO_{3-\delta}$, to prove the claimed hexagonal phase to be present here. Together with the Rietveld analysis, we are able to provide a reasonable determination of these stoichiometries. However, because an amorphous part is still present, the mass balance of the overall stoichiometry was not only reflected by the crystalline part.

A combined Rietveld/Le Bail analysis of the powder sample 2 is shown in Figure 2. The refinement converged to reliability factors of $R_{WP} = 4.72\%$ and $R_P = 3.45\%$ for the pattern with a goodness of fit = 1.25 and a Durban−Watson parameter of 1.41. The carbonate as well as spinel phases have completely vanished and have reacted towards the perovskite structures as they could not be detected by XRD in this sample.

First investigations of the XRD pattern led to the conclusion that the hexagonal perovskite simply undergoes a change

(18) De Villiers, J. P. R. *Am. Miner.* **1971**, *56*, 758.
(19) Kiseleva, L. A.; Kotelnikov, A. R.; Martynov, K. V.; Ogorodova, L. P.; Kabalov, J. K. *Phys. Chem. Miner.* **1994**, *21*, 392.
(20) Liu, X.; Prewitt, C. T. *Phys. Chem. Miner.* **1990**, *17*, 168.
(21) Gushee, B. E.; Katz, L.; Ward, R. *J. Amer. Chem. Soc.* **1957**, *79*, 5601.
(22) Taguchi, H.; Takeda, Y.; Kanamaru, F.; Shimada, M.; Koizumi, M. *Acta Crystallogr., Sect. B* **1977**, *33*, 1299.

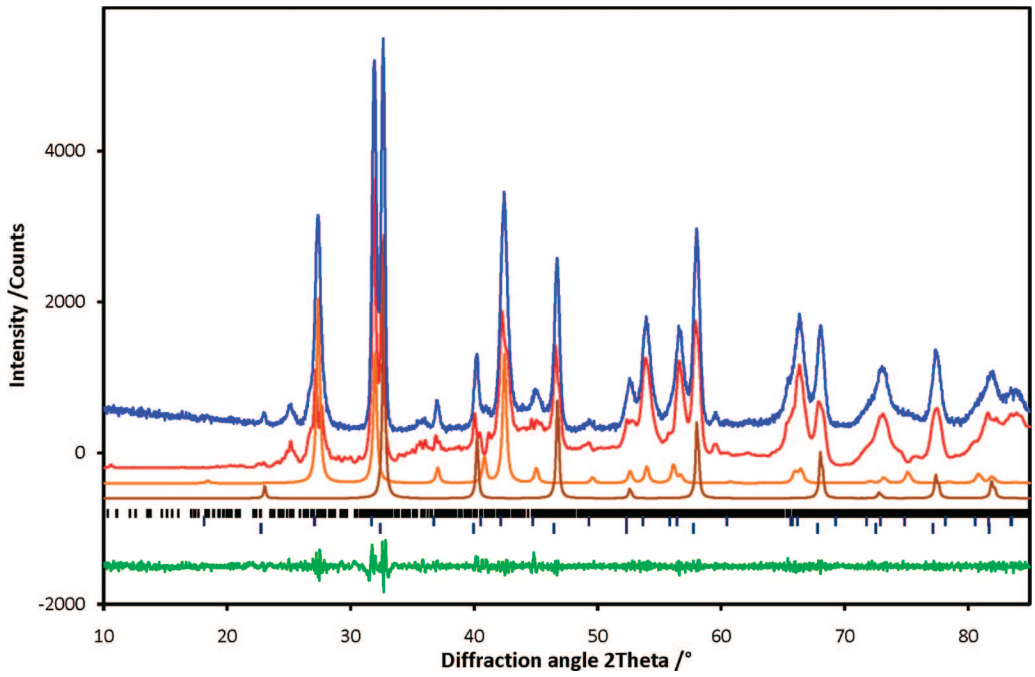


**Figure 2.** Rietveld/Le Bail plot of sample 2 ($T = 1023$ K, 10 h). The observed (blue) and calculated intensities [red, $(Ba_{0.6-x}Sr_{0.4+x})(Co_{1-y}Fe_y)O_{3-\delta}$ (monoclinic-perovskite); light brown, $(Ba_{0.6+x}Sr_{0.4-x})CoO_{3-\delta}$ (hexagonal-perovskite); brown, $(Ba_{0.25}Sr_{0.75})(Co_{0.6}Fe_{0.4})O_{3-\delta}$ (cubic-perovskite)] together with the difference (green) between the observed and calculated pattern as well as the possible reflex position (tick marks) are given.

in the lattice parameters compared with the hexagonal perovskite observed in sample 1. Attempts to refine the pattern with only the hexagonal perovskite structure together with the cubic perovskite structure failed, as well as attempts using the tetragonal structure together with the cubic structure, which was suggested by us in an earlier report.[13] We finally arrived at the conclusion that a new structure (with lower symmetry) must be formed at the expense of the hexagonal perovskite. A Le Bail whole pattern decomposition method was applied to refine the unit cell and a monoclinic unit cell (SG *P*2/*m*) with parameters obtained from the refinement in Figure 2 and shown in Table 1 was found to best fit the observed pattern. From our studies, three phases are present in powder sample 2: a cubic perovskite (~33%), a hexagonal perovskite (~33%), and a new monoclinic phase (~33%).

The hexagonal perovskite undergoes a minor change in the lattice parameters compared to those observed in powder sample 1. It must be stressed that the unit cell of the cubic perovskite did not change significantly between sample 1 and sample 2, thus leading to the conclusion that no further uptake of barium had occurred (this would have led to an increase in the unit cell parameters because the unit-cell parameters of the perovskite structures strongly depend on the radii of the A-site cation. According to Shannon,[23] $Sr^{2+} = 0.144$ nm, while $Ba^{2+} = 0.161$ nm, in the given 12-fold cuboctahedral coordination.).[13] Quantitative EDXS on a TEM, indicated that during the reaction from sample 1 to sample 2, a slight change of the A-site cation occupancy at the hexagonal site had occurred ($\text{A-site}_{\text{occupancy}} = (Ba_{0.75}Sr_{0.25})_{\text{sample1}}$ to $(Ba_{0.6+x}Sr_{0.4-x})_{\text{sample2}}$; a smooth transition between the hexagonal and the monoclinic phase is indicated by the variable $x$). This is reflected in Table 1. Further on, minor extents of iron (indicated by the variable $y$ in the stoichiometry) were found in the monoclinic phase.

Increasing the temperature leads then to a cubic perovskite structure with the reported unit cell parameter of ~0.4 nm (the data are not shown here but can be found elsewhere[13]). A summary of the reaction sequence is displayed in Figure 3. We emphasize that the presented stoichiometries of the intermediate crystalline phases are idealized and vary in certain tolerances because solid-state reactions are not static but rather dynamic processes.

To deliver further proof for the proposed reaction mechanism, an HRTEM study was conducted, combined with the quantitative EDXS results mentioned previously.

In images a and b in Figure 4, a representative HRTEM micrograph acquired for sample 1 is displayed. It shows the contact zone between a grain with cubic perovskite symmetry ($a = 0.39$ nm) viewed along the [111] zone axis (Figure 4c) and a grain with hexagonal symmetry ($a = 0.54$ nm; $c = 0.47$ nm) viewed along the [122] zones axis (Figure 4d). The hexagonal structure exhibits a slightly smaller unit cell than that found for the hexagonal cell by Rietveld analysis, as well as superlattice reflections orientated along the $[\bar{2}10]$ direction, which indicates a cation ordering along this direction as illustrated by arrows. It has to be stressed that in nanosized powder reactions, slight deviations from the macroscopic observations (XRD) may occur as the cation distribution can vary from grain to grain. Figure 5 exhibits the coexistence of the cubic perovskite ($a = 0.408$ nm) viewed along the $[01\bar{1}]$ zone axis (Figure 5b) as well as the monoclinic structure (derived from the Le Bail analysis) viewed along the [100] zone axis (Figure 5c) in sample 2. The diffraction data acquired directly from the contact zone

(23) Shannon, R. D. *Acta Crystallogr., Sect. A* **1976**, *32*, 751.

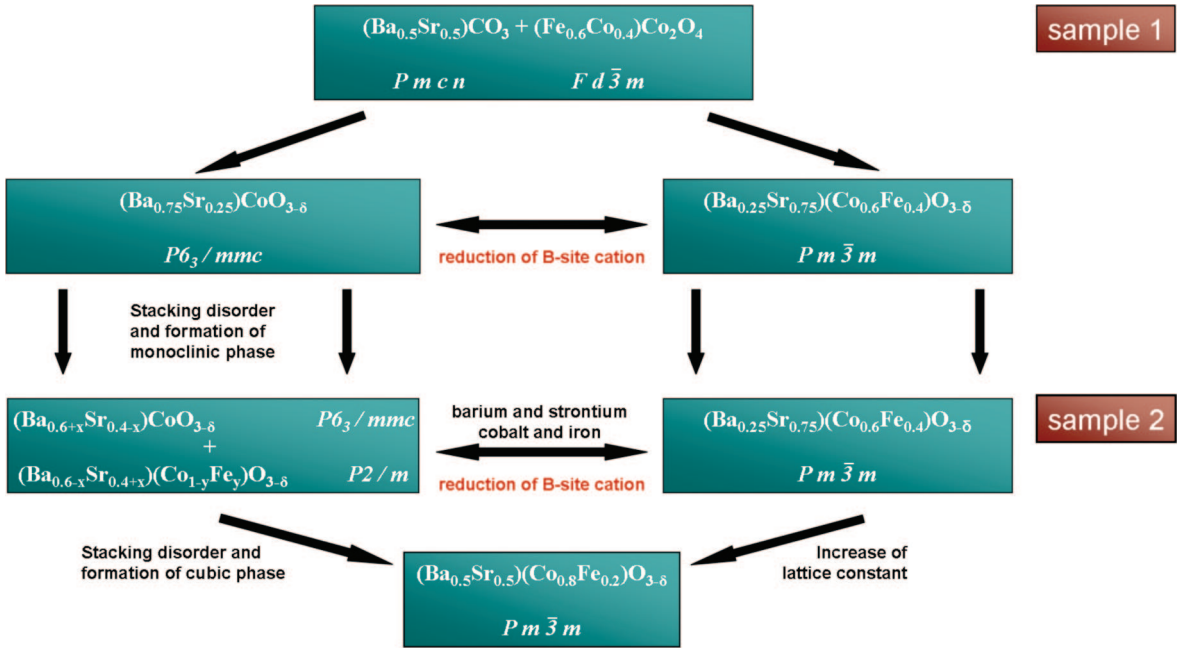


**Figure 3.** Reaction scheme of the sol−gel synthetic route of BSCF.

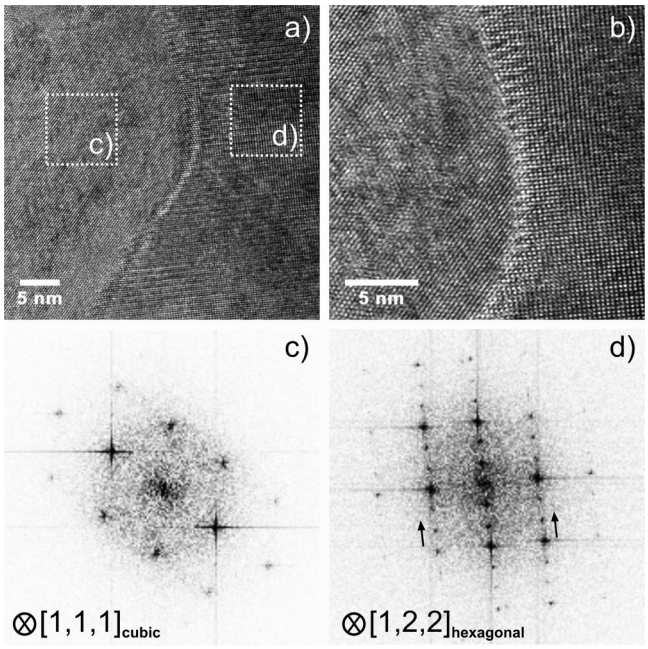


**Figure 4.** Transmission electron micrographs showing the contact zone between the cubic perovskite $(Ba_{0.25}Sr_{0.75})(Co_{0.6}Fe_{0.4})O_{3-\delta}$ (c) and the hexagonal perovskite $(Ba_{0.75}Sr_{0.25})CoO_{3-\delta}$ (d) in sample 1. (a, b) High-resolution TEM micrographs at different magnifications, (c, d) diffraction data acquired via FFT related to the marked positions in (a). Arrows in (d) indicate the direction of the cation ordering.

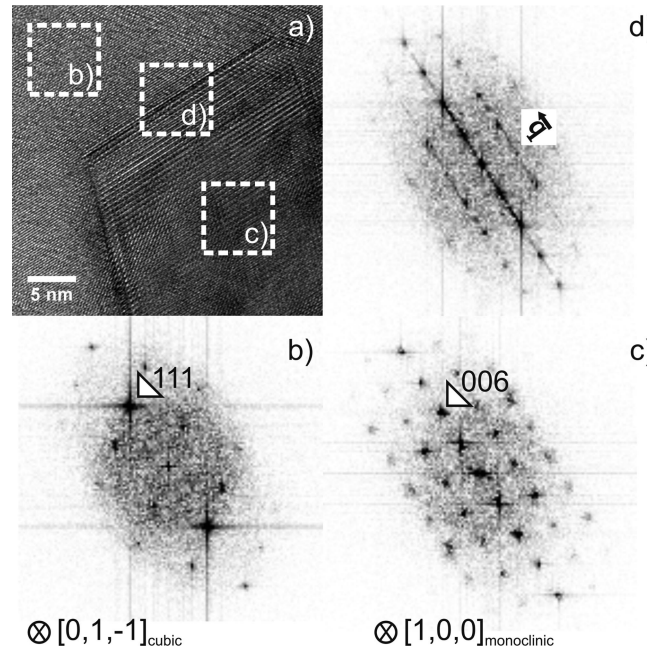


**Figure 5.** Transmission electron micrograph showing the contact zone between the cubic perovskite (b) and the monoclinic perovskite (c) in sample 2. (a) High-resolution TEM micrograph, (b−d) diffraction data acquired via FFT related to the marked positions in (a). The vector **q** (along $[003]_{monoclinic}$ and $[111]_{cubic}$) in (d)) indicates the direction of streaky intensities that are present in the vicinity of the phase boundary.

(Figure 5d) clearly shows streaky intensities. This indicates the formation of stacking disordering with a vector **q** orientated along the $(111)_{cubic}$ direction when viewed from the cubic phase and along the $(003)_{monoclinic}$ direction when viewed from the monoclinic phase. Further on, the $(111)_{cubic}$ plane is parallel to the $(006)_{monoclinic}$ plane and exhibits the same reciprocal length.

## Discussion

The work of Shao et al., Rebeilleau-Dassonneville et al., and Švarcová et al. has shown that if BSCF is kept below 1123 K for a long time period, a decomposition occurs that separates the former single cubic perovskite phase into (at least) a two-phase mixture.[3,11,12] The additional phase was referred by Shao et al. to be $BaCoO_2$. Švarcová et al. describe a 2H or 4H hexagonal structure. Rebeilleau-Dassonneville et al. also reported the decomposition into an additional phase, but here only the additional Bragg positions in the XRD pattern were given. The results of Švarcová et al. support the conclusion that a reversible process was present because they found the same phase separation in raw powders that had not been fully calcined towards the BSCF. In our

work, we also found a clear evidence for the reversibility of this process. First, we prepared a cubic BSCF powder sample and verified the phase purity by XRD. Second, we annealed this sample for 20 h at 923 K in air and re-examined phase purity by XRD. This sample already demonstrated minor contributions of the hexagonal and the monoclinic phase found in sample 1 and sample 2 as previously discussed in this report.

The main goal of this study was to identify the way the cubic perovskite is formed at the expense of the hexagonal perovskite as well as to identify the driving force for this reaction. As previously mentioned, the first reaction products of the BSCF formation are the mixed spinel $(Fe_{0.6}Co_{0.4})Co_2O_4$ and the mixed carbonate $(Ba_{0.5}Sr_{0.5})CO_3$ followed by the formation of the cubic perovskite $(Ba_{0.25}Sr_{0.75})(Co_{0.6}Fe_{0.4})O_{3-\delta}$ and the hexagonal perovskite $(Ba_{0.75}Sr_{0.25})CoO_{3-\delta}$ (see Figure 3). Because of the fact that the reaction time was set to 10 h for sample 1, it is unlikely that different diffusion kinetics yields the formation of the two different perovskites. Particularly, the separation of cobalt and iron cannot be explained by diffusion kinetics. Furthermore, a successful preparation at temperatures of $T = 1023$ K under similar reaction conditions was previously reported for $(Ba_{0.5}Sr_{0.5})(Fe_{0.8}Zn_{0.2})O_{3-\delta}$, which displays a cobalt-free cubic perovskite.[16,17,24] We therefore argue that not only diffusion kinetics are responsible for the formation of the two perovskites in the case of BSCF.

The first question that needs to be answered is why the reaction follows this particular pathway. In a simplified model, both B-site cations are assumed to be initially in a 3+ oxidation state. Though they have the same formal valence, a fundamental discrepancy between the preferred spin state of iron and cobalt has to be considered. Although $Fe^{3+}$ is mostly found in the high-spin state (octahedral oxygen environment), $Co^{3+}$ occupies equivalent sites (octahedral oxygen environment) in the low-spin state.[25−27] This fact results in huge differences in the ionic radii: $Fe^{3+}$ (HS) = 0.0645 nm and for $Co^{3+}$ (LS) = 0.0545 nm.[23] The basic discrepancy between the cubic and hexagonal perovskite is the connection of the B-site octahedra. In case of the cubic structure, only corner-sharing octahedra are present with a B−O distances of ∼0.195 nm, whereas in the hexagonal structure, face-sharing octahedral with B−O distances of ∼0.184 nm are present. Considering the large difference between the ionic radius of cobalt and iron, it is clear why cobalt prefers to form the hexagonal perovskite structure. At this point it has to be stressed that the observed B−O bonding distance clearly deviates from the sum of the effective ionic radii,[23] which can be attributed to a strong amount of covalent character in the B−O bond.[28]

The second question to be answered is why the cubic perovskite BSCF forms only above $T = 1123$ K and why it exhibits a long time stability only above this temperature. As a matter of fact, the B-site cations of perovskite-type oxides possess higher oxidation states at lower temperatures, while increasing the temperature leads to a reduction of the B-site cations.[29] This has been previously suggested by Švarcová to be the reason for the stability of the cubic perovskite at temperatures above $T = 1123$ K.[12] In other words, the decrease in the ionic radii of the B-site cations was identified to be the driving force for the formation of the hexagonal perovskite. We partly agree with this argument, but we emphasize that this is due to cobalt, which is occupying the hexagonal B-site. The redox behaviour of cubic BSCF is mainly due to cobalt.[29] Furthermore, the oxidation from $Co^{2+}$ to $Co^{3+}$ is accompanied by a change in the preferred spin state, which is the real driving force to form the hexagonal perovskite structure ($Co^{2+} = 0.0745$ nm (HS), $Co^{3+} = 0.0545$ nm (LS) compared to $Fe^{2+} = 0.0780$ nm (HS), $Fe^{3+} = 0.0645$ nm (HS)).[23]

The third question to be answered is how the reaction proceeds from the hexagonal perovskite structure towards the cubic perovskite structure, and whether there are any other structures involved that have been missed so far.

The structural relationships between the hexagonal and cubic structures were discussed already in our previous report.[13] As also described by Negas et al.,[30] it is likely that the transition from hexagonal to cubic perovskite occurs via a shear of the $AO_3$-hexagonal layers.

As mentioned above, we successfully refined the hexagonal perovskite together with the cubic perovskite structure on our powder sample 1. Švarcová et al. proposed the existence of only the hexagonal and the cubic perovskite in a powder sample that exhibits the same XRD pattern as our powder sample 2. Their results for a "raw"-powder synthesized at $T = 1023$ K and annealed samples of BSCF between 1073 and 1123 K were indexed with a hexagonal perovskite metric and showed a very similar diffraction pattern as the one reported here for our powder sample 2. However, all attempts to refine the pattern with the hexagonal perovskite and the cubic perovskite structure only failed.

Finally, a Le Bail refinement has provided evidence that sample 2 consisted of a three phase mixture containing a hexagonal, a cubic, and a monoclinic phase with unit-cell parameters shown in Table 1. To emphasize the three-phase mixture including the monoclinic phase claimed above, a refinement of sample 2 with two phase mixtures is given in Figure 6, namely hexagonal/cubic (Figure 6a) as well as tetragonal/cubic (Figure 6b). The large discrepancies are immediately clear and are visible by the difference curves. Obviously, the so far unknown intermediate monoclinic structure must be included in order to obtain probable refinement results. The creation of the monoclinic structure can be understood as described in Figure 7, where four unit cells of the hexagonal perovskite along the [001] zone axis are drawn. First, the hexagonal cell must be transformed into

(24) Feldhoff, A.; Martynczuk, J.; Wang, H. H. *Prog. Solid State Chem.* **2007**, *35*, 339.
(25) Yoon, W. S.; Kim, K. B.; Kim, M. G.; Lee, M. K.; Shin, H. J.; Lee, J. M.; Lee, J. S. *J. Phys. Chem. B* **2002**, *106*, 2526.
(26) de Groot, F. M. F.; Abbate, M.; van Elp, J.; Sawatzky, G. A.; Ma, Y. J.; Chen, C. T.; Sette, F. *J. Phys.: Condens. Matter* **1993**, *5*, 2277.
(27) Abbate, M.; Fuggle, J. C.; Fujimori, A.; Tjeng, L. H.; Chen, C. T.; Potze, R.; Sawatsky, G. A.; Eisakia, H.; Uchida, S. *Phys. Rev. B* **1993**, *47*, 16124.
(28) Goodenough, J. B.; Kafalas, J. A. *J. Solid State Chem.* **1973**, *6*, 493.
(29) Arnold, M.; Xu, Q.; Tichelaar, F.D. ; Feldhoff, F. *Angew. Chem., Int. Ed.* **2008**, submitted.
(30) Negas, T.; Roth, R. S. *J. Solid State Chem.* **1970**, *1*, 409.

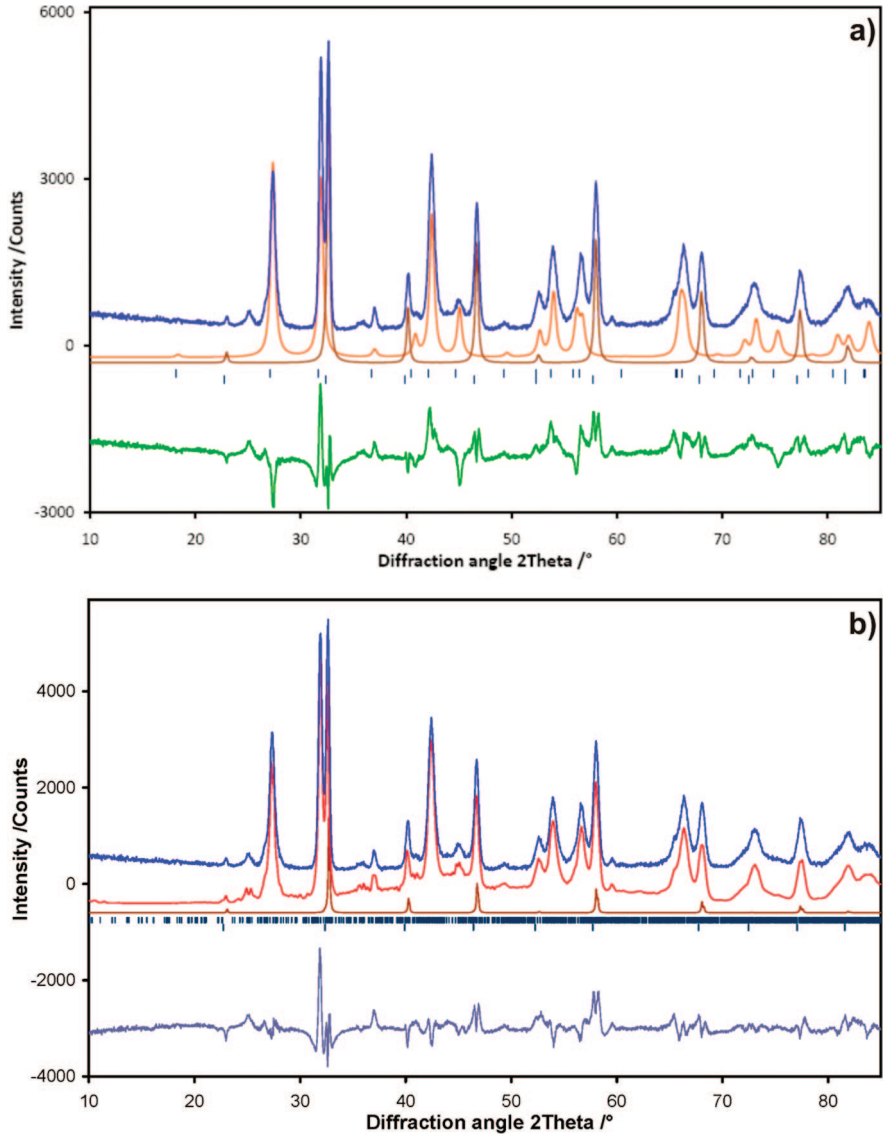


**Figure 6.** Refinement plots of sample 2 (1023 K, 10 h) refined only with the hexagonal/cubic perovskite or the tetragonal/cubic perovskite. (a) Rietveld refinement: The observed (blue) and calculated intensities [light brown, $(Ba_{0.6}Sr_{0.4})CoO_{3-\delta}$ (hexagonal-perovskite); brown, $(Ba_{0.25}Sr_{0.75})(Co_{0.6}Fe_{0.4})O_{3-\delta}$ (cubic-perovskite)] together with the difference (green) between the observed and calculated pattern as well as the possible reflex position (tick marks) are given. (b) The observed (blue) and calculated intensities [red, $(Ba_{0.6}Sr_{0.4})CoO_{3-\delta}$ (tetragonal-perovskite); brown, $(Ba_{0.25}Sr_{0.75})$ $(Co_{0.6}Fe_{0.4})$ $O_{3-\delta}$; (cubit-perovskite)] together with the difference (light-blue) between the observed and calculated pattern as well as the possible reflex position (tick marks) are given.

a pseudo-orthorhombic setting, which results in the following new unit cell parameters: $a_{hexagonal} \rightarrow a_{orthorhombic}$, $\sqrt{3} \times b_{hexagonal} \rightarrow b_{orthorhombic}$, and $c_{hexagonal} \rightarrow c_{orthorhombic}$. The monoclinic unit cell can then be approximated as a superstructure based on the pseudo-orthorhombic setting with $a_{monoclinic} = 2 \times a_{orthorhombic}$, $b_{monoclinic} = b_{orthorhombic}$, $c_{monoclinic} = 3 \times c_{orthorhombic}$. According to the assumed shearing of the hexagonal $AO_3$-layers, the superstructure is probable, particularly in the *c*-direction, which is the axis perpendicular to the stacking sequence.

A scheme of the $AO_3$-layer stacking sequence of the hexagonal and cubic perovskite is shown in Figure 8. The monoclinic stacking sequence displays an intermediate structure between these end members and a possible shift in the $AO_3$-layer stacking sequence from the hexagonal towards the cubic phase is indicated by arrows. The stacking sequence in the hexagonal perovskite is 2H, thus owing only face-sharing transition metal (TM) oxygen octahedra. Reactions toward the monoclinic cell is accompanied by a shift in some of the $AO_3$-layers, which results in a mixture of face-sharing as well as corner-sharing TM oxygen octahedra. Therefore, within the monoclinic unit cell, 3C as well as 2H stacking ordering can be observed. The final cubic BSCF perovskite is characterised by the normal 3C stacking ordering. Thus, the intermediate stacking sequence in the monoclinic cell directly reflects the intermediate valence state of the cobalt as the reaction temperature increased. As explained above, the octahedral sites in the hexagonal stacking sequence are preferably occupied by $Co^{3+}$, and the octahedral sites in the cubic stacking are preferably occupied by $Co^{2+}$. (Actually, $Co^{2.2+}$ is present at 1223 K in BSCF according to in situ electron energy-loss spectroscopy.[29]) The development of the corner-sharing octahedral sites are also in good agreement with the fact, that iron was built into the lattice during the reaction hexagonal $\rightarrow$ monoclinic because iron preferably occupies corner-sharing octahedral

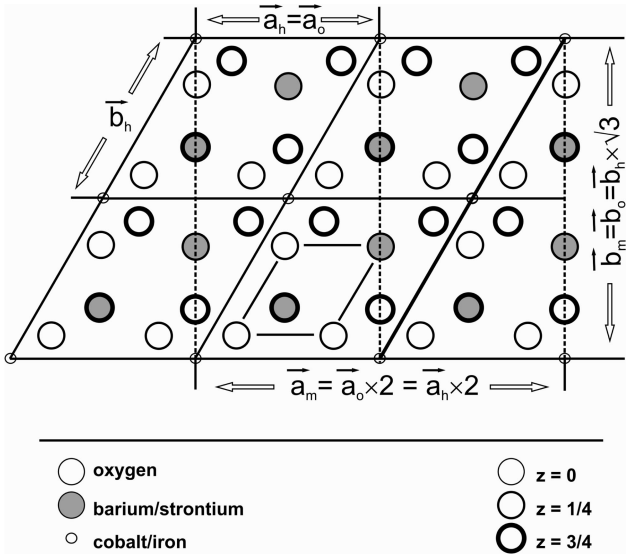


**Figure 7.** Transformation scheme of the hexagonal unit cell into the monoclinic unit cell via a pseudo-orthorhombic setting. The hexagonal unit cell is plotted along the [001] zone axis. Additionally, the $AO_3$-hexagonal layer stacking unit is highlighted.

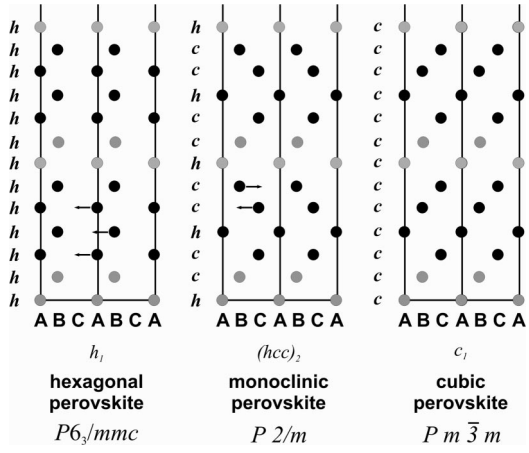


**Figure 8.** Stacking sequence of the $AO_3$-hexagonal layers in the hexagonal, monoclinic, and cubic perovskite structure. Indicated is one possible rearrangement of the stacking sequence from the hexagonal toward the cubic perovskite structure.

sites. Prolonged heating above the critical temperature of $T = 1173$ K leads to a further reordering of the stacking sequence of the monoclinic cell, which ultimately results in the cubic perovskite accompanied with an exchange of cobalt and iron and barium and strontium between these two phases, where the latter was clearly determined by in situ XRD.[13]

Further evidence for the reaction of the monoclinic towards the cubic perovskite structure is shown Figure 5d. The plane $(111)_{cubic}$ is parallel to the $(006)_{monoclinic}$ plane of the monoclinic grain with the same reciprocal length. Further on, a stacking disordering along a vector **q**, which is orientated along the $[111]_{cubic}$ direction of the cubic cell is indicated by stripes found in the diffraction data, which were acquired directly from the contact zone. This is in excellent agreement with the proposed mechanism since the stacking of the hexagonal $AO_3$-layers is perpendicular to the [111] room diagonal of the cubic perovskite. In view from the monoclinic unit cell, the stacking disordering occurs along the vector **q**, which is orientated along the $[003]_{monoclinic}$ direction. This is also in good agreement with the proposed reaction mechanism because the stacking of the hexagonal $AO_3$-layers is perpendicular to the [00l] direction of the monoclinic cell.

## Conclusions

We have presented further evidence that the decomposition of the cubic $(Ba_{0.5}Sr_{0.5})(Co_{0.8}Fe_{0.2})O_{3-\delta}$ BSCF perovskite is a process that finally separates the former cubic single phase BSCF into a two phase mixture of hexagonal and cubic perovskites, which occurs via a new monoclinic perovskite. The hexagonal perovskite was found to be a barium-rich, iron-free cobalt perovskite, whereas the cubic perovskite was identified to be a strontium-rich, iron-cobalt perovskite.

Furthermore, our results deliver arguments that the main driving force for this reaction is the oxidation of the B-site cobalt ion, which preferably occupies the low-spin state, if oxidized to states close to 3+. This enforces the formation of a hexagonal perovskite with small B−O bonding distances. Additionally, we identified a reordering of the stacking sequence of the hexagonal perovskite that can lead to the cubic perovskite or backwards to the hexagonal perovskite. During this reaction, a so far unknown monoclinic phase was formed, which was found to be a superstructure based on the hexagonal perovskite. These results deliver the explanation as to why and how particularly cubic cobalt perovskites tend to segregate into hexagonally stacked perovskites at intermediate temperatures.

**Acknowledgment.** The authors greatly acknowledge financial support from the DFG (Grant FE 928/1-2) and fruitful discussions with Professor Jürgen Caro.

CM801463H